sciendo

LATVIAN JOURNAL OF PHYSICS
AND TECHNICAL SCIENCES
2024, N 2

DOI: 10.2478/lpts-2024-0015

TOWARDS HIGH-PRECISION QUADROTOR TRAJECTORY FOLLOWING CAPABILITIES: MODELLING, PARAMETER ESTIMATION, AND LQR CONTROL

A. Hanif, I. E. Putro*, A. Riyadl, O. Sudiana, Hakiki, H. Y. Irwanto

Research Organization for Aeronautics and Space,
National Research and Innovation Agency (BRIN),
Jakarta 10340, INDONESIA
*e-mail: idris.eko.putro@brin.go.id

Quadrotor unmanned aerial vehicles (UAVs) are small, agile four-rotor systems suitable for various applications, from surveillance to disaster support missions. Hence, achieving high-precision trajectory tracking is crucial for their successful deployment. This research focuses on modelling, parameter identification, and Linear Quadratic Regulator (LQR) control design for quadrotors, aiming to enhance their trajectory following capabilities. The quadrotor dynamics are a sixth degree-of-freedom (6DOF) equation of motion derived from Newton's second law, encompassing moment of inertia, centre of gravity, weight, and thrust of propeller parameters. Experimental measurements are conducted to accurately determine these parameters, ensuring a realistic representation of the quadrotor system. Subsequently, a linearized model is constructed to provide a suitable plant for control system development. The LQR control design is intended to improve the trajectory tracking performance. This control strategy is validated through simulation and practical experiments, demonstrating its effectiveness in achieving high-precision trajectory following capabilites. The proposed approach demonstrates that LQR control effectively guides the quadrotor to resemble a predefined trajectory, experiencing only 3 % overshoot observed during the initial phase of flight.

Keywords: *Control, LQR, modelling, parameter estimation, quadrotor, unmanned aerial vehicles (UAVs).*

1. INTRODUCTION

Autonomous unmanned aerial vehicles (UAVs), particularly quadrotors, have garnered significant interest due to their versatility and wide-ranging applications. Quadrotors are agile, four-rotor systems with VTOL capabilities, making them suitable for tasks such as surveillance, remote inspection, disaster management [1], and defense missions. Precise control is essential for quadrotors, given their waypoint and trajectory following missions [2].

Linear Quadratic Regulator (LQR) control methods have gained prominence in quadrotor control system design. Previous research [3] focused on LQR controller design for quadrotor helicopters and performance analysis. Another study [4] used a modified LQR approach to tune a PID controller's parameters based on experimental model parameter values. This modification introduced feedback considering the tracking error between the state vector and a reference state vector.

Furthermore, LQR has been employed to minimize steady-state errors and overshoot in waypoint following for flying wing UAVs [5]. Comparisons between LQR and other control methods, such as PID, PD, model predictive control (MPC), feedback linearization (FL), and sliding mode control (SMC), have been explored in various studies [6]–[10], often focusing on position and attitude control. These comparisons have provided insights into the effectiveness of different control strategies, including fuzzy logic and model reference adaptive PID controllers (MRAC) based on the MIT rule.

This paper explores quadrotor modelling and control design for precise trajectory following, employing LQR methodology. The model is developed to exhibit quadrotor dynamics, validated using flight test data and augmented with parameter estimation to enhance the precision of quadrotor UAVs in trajectory tracking.

2. PARAMETER ESTIMATION

The experimental measurement of quadrotor components must be conducted to estimate the right parameters and govern the dynamic equations.

2.1. Quadrotor Configuration

Quadrotor configuration can be depicted from Fig. 1 and Table 1.

Table 1. Quadrotor Specifications

Parameter	Value	Unit	Parameter	Value	Unit
Height	9.5	cm	Payload Capacity	0.15	kg
Length	38	m	Arm length	0.19	m
Mass	0.5	kg	COG position	0.05	m
Blade Span	10	cm	Number of blades	2	



Fig. 1. Quadrotor UAV.

The modelling of quadrotor follows necessary assumption, i.e., the quadrotor structure is supposed to be rigid and symmetrical, centre of gravity coincides with the body-fixed frame, and there is no mechanical and electrical characteristics difference between each brushless-motor, and also the quadrotor inflow is steady and uniform.

2.2. Moment of Inertia

To derive the moment and products of inertia for a small quadrotor, two methods are available: experimental measurement and theoretical calculation. While experiments yield real quadrotor values and are more accurate, they can be complex and costly for full-scale quadrotors. As a practical alternative, theoretical calculation is preferred. This approach involves modelling the quadrotor as cuboids and applying the parallel axis theorem [11]–[13], as illustrated in Fig. 2:

$$I_{xx} = I_{yy} = 2m(1+L)^2 + \frac{1}{12}M\left(c^2 + b^2\right) + M\left(\frac{c}{2}\right)^2, \tag{1}$$

$$I_{zz} = 4m(1+L)^2 + \frac{1}{12}M\left(a^2 + b^2\right), \tag{2}$$

$$I_{xy} = I_{xz} = I_{yz} = 0, \tag{3}$$

where M is the total mass of battery, quadrotor frame (at length l), and payload systems. Variable m denotes summation mass of quadrotor frame (from length l to L) and individual motor system. The dimensions of masses and lengths are presented in Table 2.

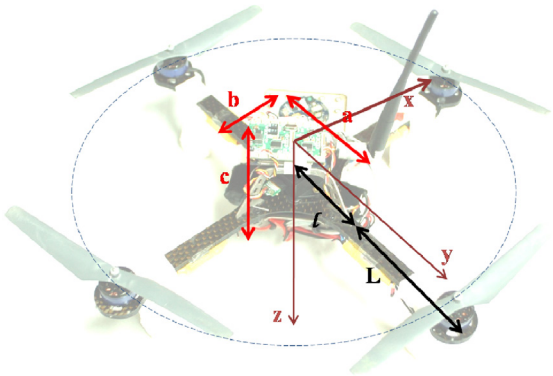


Fig. 2. Free body diagram simplified quadrotor model for inertia moment estimation.

Table 2. Masses and Lengths of Quadrotor

Parameter masses	Value	Unit	Parameter length	Value	Unit
Motor BLDC+Blade+Speed controller	4 x 0.047	kg	a	0.075	m
Battery system	0.1	kg	b	0.07	m
Payload (Sensor+Accuisition Board)	0.05	kg	c	0.07	m
Frame	1.70	kg	l	0.06	m
			L	0.019	m

By using the parallel axis theorem approach, we obtain the inertial moment values as shown in Table 3.

Table 3. Moment of Inertial Values Using Theoretical Approach

Parameter	Value	Unit
I_{xx}	4.82 x 10^{-3}	kg.m^2
I_{yy}	4.82 x 10^{-3}	kg.m^2
I_{zz}	8.77 x 10^{-3}	kg.m^2

2.3. Rotary Wing Motor

The quadrotor's electric propulsion system, consisting of a propeller, BLDC motor, and electronic speed controller, is essential for its control. Unlike manned aerial vehicles controlled by a joystick pilot, quadrotors receive angular propeller motion (RPM) in unmanned systems. Therefore, it is crucial to create a rotor model that accurately relates joystick inputs to motor dynamics.

To develop the motor model, experiments are conducted, collecting data from joystick command inputs and correlating them with propeller speed responses. These data enhance the accuracy of rotor simulations. Figure 3 outlines the experimental setup for the motor model development.

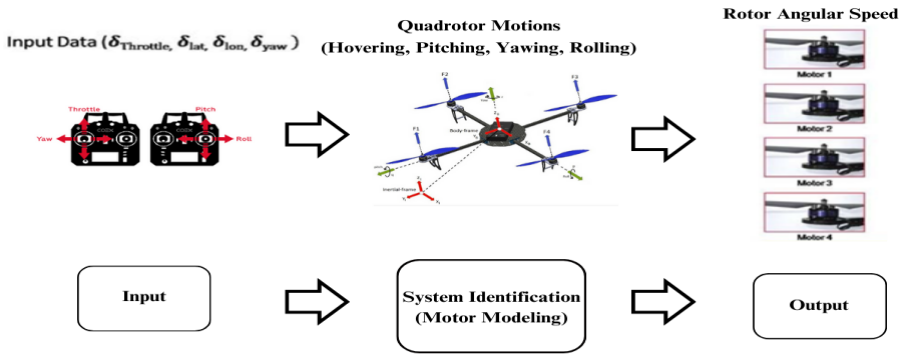


Fig. 3. Experimental process for motor identification.

Experiments are conducted to collect the data for roll and pitch dynamics; thus, rotor identification can be developed and validated consecutively. Figure 4 shows joystick input inserted to the BLDC motor for roll dynamics.

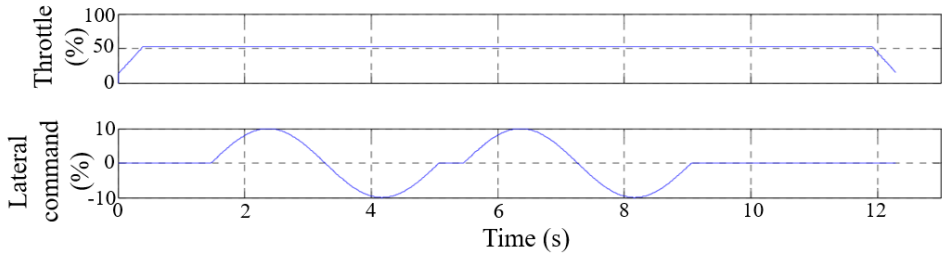


Fig. 4. Joystick inputs for roll dynamics.

The collective command $\delta_{throttle}$ to be set to a constant value and the lateral command δ_{lat} are sent to change the dynamic in rolling motion. Meanwhile, the other commands (δ_{long} and δ_{yaw}) are idle. The motor responses can then be acquired and compared to the validation results. Figures 5 and 6 depict the front side and right side of BLDC motor responses for roll dynamics.

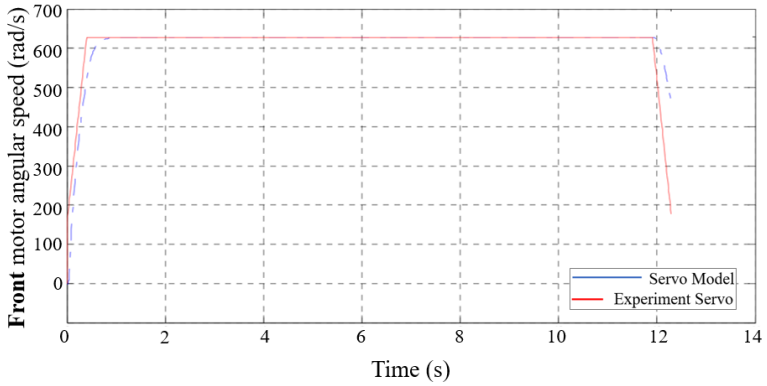


Fig. 5. Front side of the motor responses for roll dynamics.

Figures 5 and 6 show that both the front and right side of the motor responses of the quadrotor resemble the experiment data.

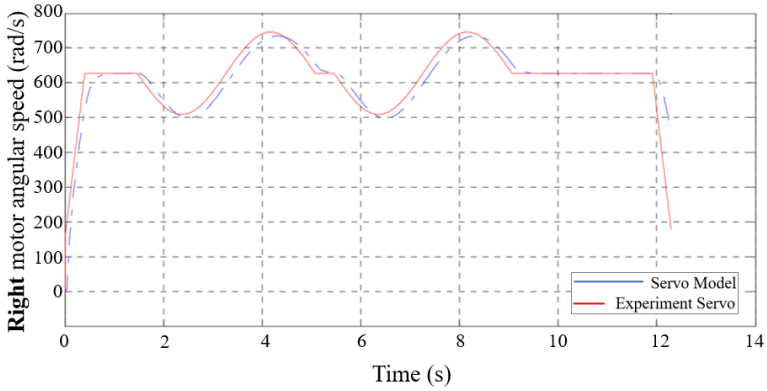


Fig. 6. Right side of the motor responses for roll dynamics.

The motor dynamics model closely approximates real motor behaviour with minimal error, accurately representing the rotor system. The left and right motors exhibit similar responses, though in opposite directions, due to the symmetrical configuration of all motors.

The same behaviour of the rotor system is obtained for pitch dynamic. Parameter identification of pitch dynamic for the rotor model requires $\delta_{throttle}$ to be set to a constant value, and the longitudinal command δ_{long} is sent to change of the motion. The other commands (δ_{lat} and δ_{yaw}) remain idle. In pitch dynamic, the right and left sides of BLDC responses are similar to front side motor in roll dynamics as shown in Fig. 5. They maintain their speeds together to produce enough thrust for pitch motion. Meanwhile, the dynamics of the front and rear sides of the motor angular speeds in pitch dynamics cause the change in pitch motion. Due to the symmetrical configuration, the front and rear motors exhibit similar responses as in Fig. 6, though in opposite directions between right and left sides. The rotor dynamic models resemble real motors in experiments with small errors. Hence, this rotor model is precise enough to represent the real rotor system in lateral and longitudinal modes.

3. QUADROTOR MODELLING

3.1. Quadrotor Dynamics

The nonlinear behaviour of quadrotor can be represented by 6DOF equation of motions. The equation of motion for a small quadrotor with respect to earth coordinate system is presented in this section.

For translational motion, the EOM is shown as Eq. (4) to Eq. (6):

$$\ddot{x} = \frac{1}{m}(\cos\psi \sin\theta \cos\varphi + \sin\psi \sin\varphi)\sum_{i=1}^{4} T_i + \frac{1}{m}\sum_{i=1}^{4} H_{x_i}\ ; \tag{4}$$

$$\ddot{y} = \frac{1}{m}(\sin\psi \sin\theta \cos\varphi + \cos\psi \sin\varphi)\sum_{i=1}^{4} T_i + \frac{1}{m}\sum_{i=1}^{4} H_{Y_i} ; \tag{5}$$

$$\ddot{z} = g - (\frac{1}{m}\cos\theta\cos\varphi\sum_{i=1}^{4} T_i) . \tag{6}$$

While rotational EoM is shown as Eq. (7) to Eq. (9):

$$\ddot{\varphi} = \dot{\theta}\frac{\dot{\psi}(I_{yy} - I_{zz})}{I_{xx}} + \frac{1}{I_{xx}}(T_4 - T_2) + (\sum_{i=1}^{4} H_{x_i})\frac{h}{I_{xx}} + \frac{R_{x_1} - R_{x_2} + R_{x_3} - R_{x_4}}{I_{xx}} ; \tag{7}$$

$$\ddot{\theta} = \dot{\varphi}\frac{\dot{\psi}(I_{zz} - I_{xx})}{I_{yy}} + \frac{1}{I_{yy}}(T_3 - T_1) + (\sum_{i=1}^{4} H_{y_i})\frac{h}{I_{yy}} + \frac{R_{y_1} - R_{y_2} + R_{y_3} - R_{y_4}}{I_{yy}} ; \tag{8}$$

$$\ddot{\psi} = \dot{\varphi}\frac{\dot{\theta}(I_{xx} - I_{yy})}{I_{zz}} + \frac{1}{I_{zz}}(\tau_1 - \tau_2 + \tau_3 - \tau_4) + (H_{x_4} - H_{x_2})\frac{1}{I_{zz}} + (H_{x_3} - H_{x_1})\frac{1}{I_{zz}} ; \tag{9}$$

where

$$T = C_T \rho A(\Omega R_{rad})^2 ; \tag{10}$$

$$H = C_H \rho A(\Omega R_{rad})^2 ; \tag{11}$$

$$Q = C_Q \rho A(\Omega R_{rad})^2 R_{rad} ; \tag{12}$$

$$Q = C_Q \rho A(\Omega R_{rad})^2 R_{rad} ; \tag{13}$$

$$\frac{C_T}{\sigma a} = \left(\frac{1}{4} + \frac{1}{4}\mu^2\right)\theta_0 - \left(1 + \mu^2\right)\frac{\theta_{tw}}{8} - \frac{1}{4}\lambda ; \tag{14}$$

$$\frac{C_H}{\sigma a} = \left(\frac{1}{4a}\mu\overline{C}_d\right) + \frac{1}{4}\lambda\mu\left(\theta_0 - \frac{\theta_{tw}}{2}\right); \tag{15}$$

$$\frac{C_Q}{\sigma a} = \frac{1}{8a}\left(1 + \mu^2\right)\overline{C}_d + \lambda\left(\frac{1}{6}\theta_0 - \frac{\theta_{tw}}{8} - \frac{1}{4}\lambda\right); \tag{16}$$

$$\frac{C_{R_m}}{\sigma a} = -\mu\left(\frac{1}{6}\theta_0 - \frac{\theta_{tw}}{8} - \frac{1}{8}\lambda\right). \tag{17}$$

Quadrotor is equipped with four fixed-rotors consisting of a brushless DC motor and propellers. This rotor system can be described using well-known equations [14]:

$$L\frac{di}{dt} = \delta - R_{mot} i - k_m \omega_m ; \tag{18}$$

$$J_m \frac{d\omega_m}{dt} = \tau_m - \tau_d . \tag{19}$$

Second order motor dynamics can be derived by assuming the used motor is small enough; thus. it has a very low inductance

$$J_m \frac{d\omega_m}{dt} = -\frac{k_m^2}{R_{mot}}\omega_m - \tau_d + \frac{k_m}{R_{mot}}\delta . \tag{20}$$

3.2. Linearized Model

Linearization is employed to obtain a linear model that approximates the quadrotor behaviour around trim condition, refers to a specific set of operating conditions. Linearization is performed using Taylor series expansion or Jacobian matrices to approximate the nonlinear equations as a set of linear equations that describe small perturbations from the chosen operating point. These linear models approximate how the quadrotor's state variables such as position, attitude, and velocity evolve in response to control inputs when the system is close to the trim condition.

A trimmed flight condition is defined as a state where the system is in balanced, steady-state with no rate of change and the resultant forces and moments are zero [15]:

$$f(x_e, u_e) = 0, \tag{21}$$

where x_e is an equilibrium value of state vector and u_e is a control vector in an equilibrium flight condition. The small perturbation is implemented to the trim condition; thus, the total state of each motion variable is equal to the sum of a steady state (equilibrium flight due to trimmed condition before) quantity and a perturbed state quantity [16]. The linearized model of a quadrotor can be written in the state space form as follows:

$$\dot{x} = Ax(t) + Bu(t), \tag{22}$$

where $x(t)$ is a state variable, $u(t)$ is control variable, A and B are system matrix and matrix input.

In terms of quadrotor dynamics, we can describe a state variable as follows:

$$x = \begin{bmatrix} u & v & w & p & q & r & \varphi & \theta & \psi \end{bmatrix}^T. \tag{23}$$

Control variable is described as follows:

$$u = \begin{bmatrix} \delta_{lat} & \delta_{long} & \delta_{yaw} & \delta_{throttle} \end{bmatrix}^T. \tag{24}$$

Matrix A and B are shown in the following form:

$$A = \begin{bmatrix} X_u & 0 & 0 & 0 & 0 & 0 & X_\varphi & X_\theta & X_\psi \\ 0 & Y_v & 0 & 0 & 0 & 0 & Y_\varphi & Y_\theta & Y_\psi \\ 0 & 0 & Z_w & 0 & 0 & 0 & Z_\varphi & Z_\theta & 0 \\ 0 & 0 & 0 & 0 & X_u & X_u & 0 & 0 & 0 \\ 0 & 0 & 0 & X_u & X_u & X_u & 0 & 0 & 0 \\ 0 & 0 & 0 & 0 & 0 & 0 & 0 & 0 & 0 \\ 0 & 0 & 0 & 1 & 0 & 0 & 0 & 0 & 0 \\ 0 & 0 & 0 & 0 & 1 & 0 & 0 & 0 & 0 \\ 0 & 0 & 0 & 0 & 0 & 1 & 0 & 0 & 0 \end{bmatrix}; \tag{25}$$

$$B = \begin{bmatrix} X_{lat} & X_{long} & X_{ped} & X_{col} \\ Y_{lat} & Y_{long} & Y_{ped} & Y_{col} \\ Z_{lat} & Z_{long} & Z_{ped} & Z_{col} \\ L_{lat} & L_{long} & L_{ped} & L_{col} \\ M_{lat} & M_{long} & M_{ped} & M_{col} \\ N_{lat} & N_{long} & N_{ped} & N_{col} \\ 0 & 0 & 0 & 0 \\ 0 & 0 & 0 & 0 \\ 0 & 0 & 0 & 0 \end{bmatrix}. \tag{26}$$

In this research, the quadrotor is linearized in two modes: hover flight and forward flight. The operating point used for linearization in hover condition is set for translation rates and angular rates close to zero, hence:

$$u = 0 \quad p = 0 \quad \varphi = 3.2x10^{-4}\, rad$$
$$v = 0 \quad q = 0 \quad \theta = -1.5x10^{-5}\, rad$$
$$w = 0 \quad r = 0 \quad \psi = 1.67x10^{-8}\, rad$$

While in forward flight, the operating point used is in cruise condition:

$$u = 2m/s \quad p = 0 \quad \varphi = 0.1rad$$
$$v = 0m/s \quad q = 0 \quad \theta = 0.1rad$$
$$w = 0m/s \quad r = 0 \quad \psi = 0.1rad$$

A comparison of linear and nonlinear models is presented in Fig. 7.

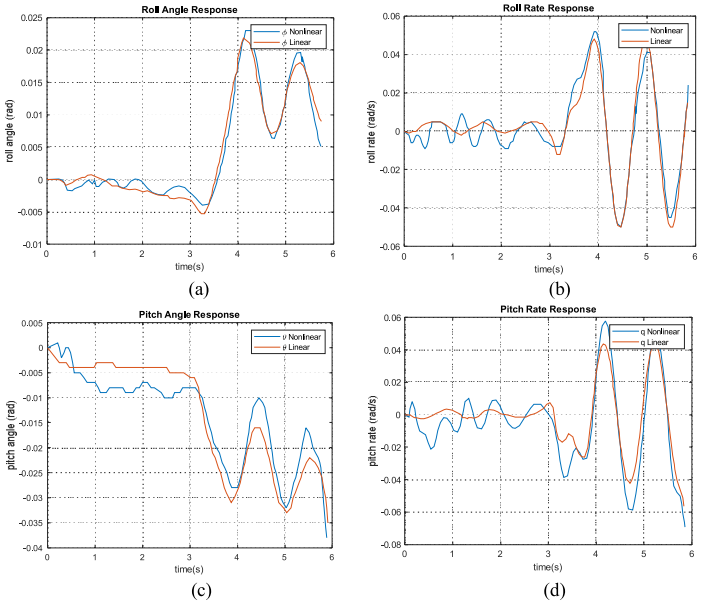


Fig. 7. Linear model validation: (a) roll angle, (b) roll rate, (c) pitch angle, (d) pitch rate.

The blue line on the graph denotes linear model responses, while the red line signifies nonlinear model responses. The linear model of the quadrotor resembles the nonlinear model; hence, the linear model can represent the nonlinear model to be utilized for optimal control system design.

3.3. Stability Augmentation System (SAS) Model

The quadrotor is inherently unstable due to nonlinear behaviour, cross-coupling in dynamics, and lightweight, so it is sensitive to external disturbances. The engineers then

come up with particular controls to solve this unstable performance. They develop a control system to maintain the quadrotor vehicle having angular attitudes that tend to zero in hover condition. This control algorithm tries to keep rotational motion such as roll, pitch, and yaw in very small angles ($[\varphi \quad \theta \quad \psi]^T \cong 0$ and its angular rate in zero rate of changes ($[\dot{\varphi} \quad \dot{\theta} \quad \dot{\psi}]^T \cong 0$. Using this kind of control system, the quadrotor attitude will be stable, so the hovering flight can be obtained without paying excessive attention. Moreover, it is also robust for any small disturbances, such as wind inside the room and noise at the joystick command. The successful controller, which guarantees the small quadrotor can be flown in stable condition, is commonly known as Stability Augmentation System (SAS Controller).

The SAS controller used on this quadrotor vehicle follows the equation below:

$$\delta_{sas_n}(t) = K_i * \int_0^t e_n(t) + K_p * e_n(t) + K_d * \frac{de_n(t)}{dt} + K_{pr} * e_{nr}(t), \tag{27}$$

where $\delta_{sas_n}(t)$ denotes an input for quadrotor motor (%), $e_n(t)$ is attitude errors (rad), $e_{nr}(t)$ is rate gyro errors (rad/s), K_{pr} is a proportional gain for rate attitude, K_p, K_i, and K_d are PID gain for integral, proportional, and differential, respectively.

Equation above is combined with the signal from joystick to give command input for quadrotor motions. Unless for throttle deflection, the other command inputs will be augmented by SAS as the following equation:

$$U_{(2,3,4)}(t) = \delta_{(lateral,long,heading)}(t) + \delta_{sas_roll}(t). \tag{28}$$

4. LQR DESIGN

4.1. Linear Quadratic Regulator (LQR)

Given the system dynamics equation,

$$\dot{x} = Ax + Bu. \tag{29}$$

The LQR method finds the optimal control decision by considering the system states and control input. The optimal controller is obtained by using the state feedback gain that minimizes a quadratic cost function.

$$J = \int_0^\infty \left(x^T Q x + u^T R u\right) dt. \tag{30}$$

The weighting matrix Q determines which states will be controlled more tightly than others. Weighting matrix R weights the control input movement that needs to be applied depending on how large the state deviates. Then, the optimal gain matrix K can be acquired using the following equation:

$$K = R^{-1} B^T P, \tag{31}$$

where P is obtained by solving algebraic Riccati equation (ARE) as:

$$A^T P + PA - PBR^{-1} - B^T P + Q = 0. \tag{32}$$

4.2. Trajectory Tracking Control

The LQR method can be utilised for designing trajectory following control, which is a tracking problem control. The principle of this tracking problem is to compare the output y(t) to a reference r(t) and expected to follow the given reference [17]. LQR will minimize the error between the output and the given reference.

$$y_{error}(t) = x_{error}(t) = x_{ref}(t) - x(t). \tag{33}$$

Conducting the time derivative of the equation yields

$$\dot{x}_{error}(t) = \dot{x}_{ref}(t) - \dot{x}(t). \tag{34}$$

Setting the reference as a constant, the equation is simplified as:

$$\dot{x}_{error}(t) = -\dot{x}(t). \tag{35}$$

Trajectory following controller design takes the following expression:

$$\dot{x}_{error}(t) = -\gamma\dot{x}(t); \gamma = 1,2,..,n, \tag{36}$$

where γ is an arbitrary positive constant representing the weight of the tracking performance in the cost function. The tracking error matrix $x_{error}(t)$ can be written in matrix form as:

$$x_{error}(t) = \begin{bmatrix} x_{error}(t) \\ y_{error}(t) \\ z_{error}(t) \end{bmatrix} = \begin{bmatrix} x_{ref}(t) - x(t) \\ y_{ref}(t) - y(t) \\ z_{ref}(t) - z(t) \end{bmatrix}, \tag{37}$$

where x, y, and z are the positions of the vehicle in the body axis frame. Derivation of the equation above can be written as:

$$\dot{x}_{error}(t) = \begin{bmatrix} \dot{x}_{error}(t) \\ \dot{y}_{error}(t) \\ \dot{z}_{error}(t) \end{bmatrix} = \begin{bmatrix} -\gamma\dot{x}(t) \\ -\gamma\dot{y}(t) \\ -\gamma\dot{z}(t) \end{bmatrix}. \tag{38}$$

Comparing with the state variable of state space system $\left([\dot{x} \quad \dot{y} \quad \dot{z}]^T\right) = \left([u \quad v \quad w]^T\right)$, the equation above can be formed to be

$$\dot{x}_{error}(t) = -\begin{bmatrix} \gamma u(t) \\ \gamma v(t) \\ \gamma w(t) \end{bmatrix}. \tag{39}$$

Due to error state vectors appearing, the state space system of the quadrotor model must be adjusted in order to accommodate the trajectory following mission as below:

$$\dot{x}_{adj}(t) = A_{adj}x_{adj}(t) + B_{adj}u_{adj}(t), \tag{40}$$

where subscript "adj" denotes the adjusted variable that will be included in the existing state space model of the quadrotor. The adjusted matrices are defined as:

$$x_{adj} = [x_{error} \quad y_{error} \quad z_{error} \quad x]^T, \tag{41}$$

$$A_{adj} = \begin{bmatrix} 0_{3x3} & -\gamma I_3 & 0_{3x(n-3)} \\ 0_{nx3} & A_{nxn} & \end{bmatrix}^T, \tag{42}$$

$$B_{adj} = \begin{bmatrix} 0_{3x4} \\ B_{nx4} \end{bmatrix}^T, \tag{43}$$

where n is the amount of state vector in the state space model. The quadratic cost function then can be written as the following expression:

$$J = \int_{t_0}^{t_f} \left(x^T{}_{adj} Q x_{adj} + u^T R u\right) dt. \tag{44}$$

5. SIMULATION RESULT

This section explains model validation and control simulation results. The validation prioritizes comparisons between nonlinear models and flight test data, as well as SAS model. This validation assures that the linear model obtained from the nonlinear model is correct, allowing for precise control design.

5.1. Nonlinear Model Validation

The nonlinear model, as the full quadrotor model, is validated using experimental data generated from flight tests. The flight test has to record proper input and output data. The inputs are Joystick inputs, and the outputs are the behaviours of the quadrotor, which are measured by various sensors.

$$u_{\exp} = \left[\delta_{throttle} \quad \delta_{lat} \quad \delta_{long} \quad \delta_{heading}\right]^T, \tag{45}$$

$$Y_{\exp} = \left[\varphi \quad \dot{\varphi} \quad \theta \quad \dot{\theta} \quad \psi \quad \dot{\psi} \quad h\right]^T, \tag{46}$$

where the command inputs consist of the throttle input $\delta_{throttle}$, the lateral input δ_{lat}, the longitudinal input δ_{lon}, and the heading input $\delta_{heading}$. The variable outputs consist of angular motions $\left(\varphi \quad \theta \quad \psi\right)$ from IMU, angular rates $\left(\dot{\varphi} \quad \dot{\theta} \quad \dot{\psi}\right)$ from rate-gyro, and altitude (h) from ultrasonic sensor.

Table 4. Flight Condition for Validation

Flight parameters	Trim condition	Flight parameters	Trim condition
Roll, φ (rad)	1.77E-4	X – position, *x* (m)	0
Roll rate, $\dot{\varphi}$ (rad/s)	0.004	X – velocity, *u* (m/s)	-0.015
Pitch, θ (rad)	0.001	Y – position, *y* (m)	0
Pitch rate, $\dot{\theta}$ (rad/s)	0.003	Y – velocity, *v* (m/s)	0
Yaw, ψ (rad)	3.398	Z – position, *z* (m)	0
Yaw rate, $\dot{\psi}$ (rad/s)	-0.003	Z – velocity, *w* (m/s)	0

Nonlinear model simulation and flight test simulation validation are conducted in the hover condition. Therefore, the inner-loop controller is set to keep the attitude dynamics of the quadrotor relatively stable and maintain the altitude. The flight conditions used for the quadrotor model simulation are shown in Table 4.

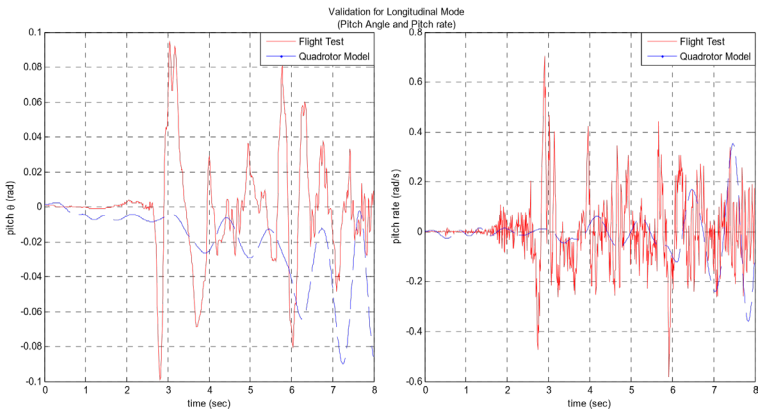


Fig. 8. Nonlinear model validation compared to flight test data for pitch dynamic.

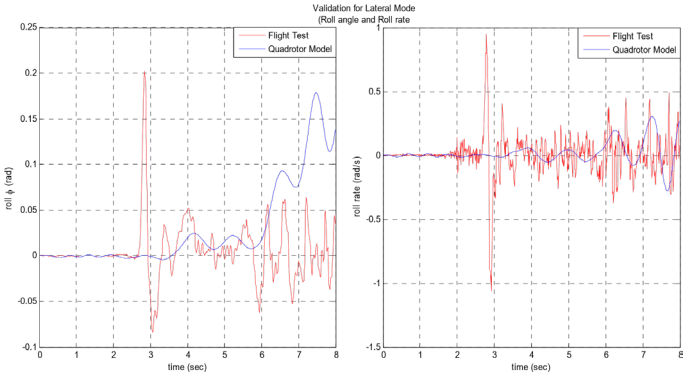


Fig. 9. Nonlinear model validation compared to flight test data for roll dynamic.

Quadrotor model validation compared to flight test responses are presented in Fig. 8 for longitudinal mode, and Fig. 9 for lateral mode.

Figures 8 to 9 depict that the responses of the quadrotor model resemble the flight test for pitch rate and roll rate. The responses of the model for pitch and roll are disparate from the flight test.

5.2. Trajectory Following Control Simulation

This control design uses LQR approach since this method is capable of reducing the quadrotor response settling time and overshoot percentage. The weighting matrices R and Q are set as uniform diagonal matrices with different values. Table 5 shows various LQR configurations.

Based on Table 5, configuration No. 3 is chosen because it is optimal for the quadrotor, considering the settling time and overshoot percentage. The result of the seventh configuration is presented in Fig. 10 for translational motion and Fig. 11 for rotational motion. Figures 10 and 11 depict that the LQR manages to converge the output states to 0. The trajectory following control is presented in Fig. 12 (a) for the circular path and Fig. 12 (b) for the spiral path.

Table 5. Various LQR Configurations

No.	Q	R	Settling time *ts* (second)		W overshoot
			Translation	Rotation	
1.	10	1	250	>1000	180 %
2.	1000	1	173	550	5 %
3.	100	0.01	150	7	2.5 %

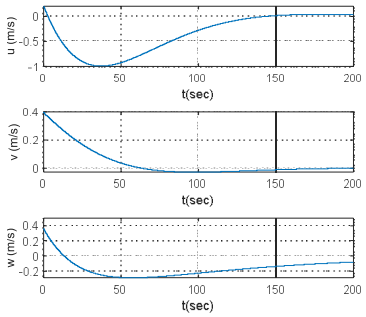


Fig. 10. Translational motion result of the seventh LQR configuration.

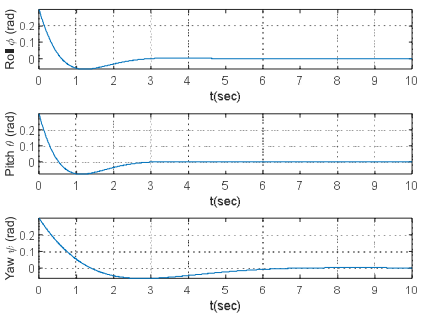


Fig. 11. Rotational motion result of the seventh LQR configuration.

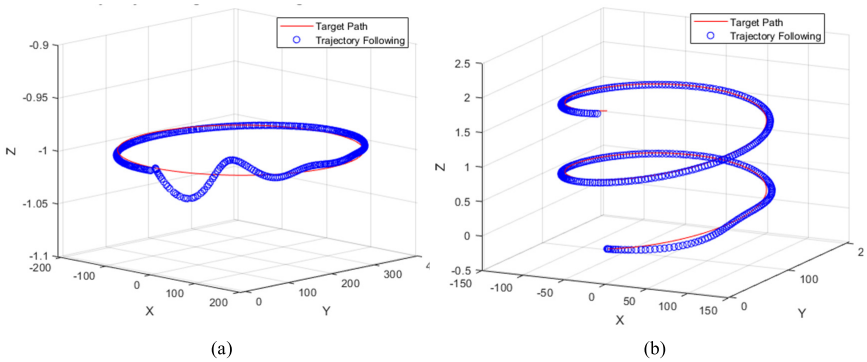


Fig. 12. Trajectory following simulation of quadrotor (a) circular path and (b) spiral path.

Figure 12 shows that the model can resemble the trajectory command given. There is a deviation at the beginning of the simulation, but it is tolerable since it is only 3 %. Deviation occurs because the model has a long settling time to recover steady state. The velocity and position profiles are presented in Fig. 13 as the supporting details of whether the deviation happens.

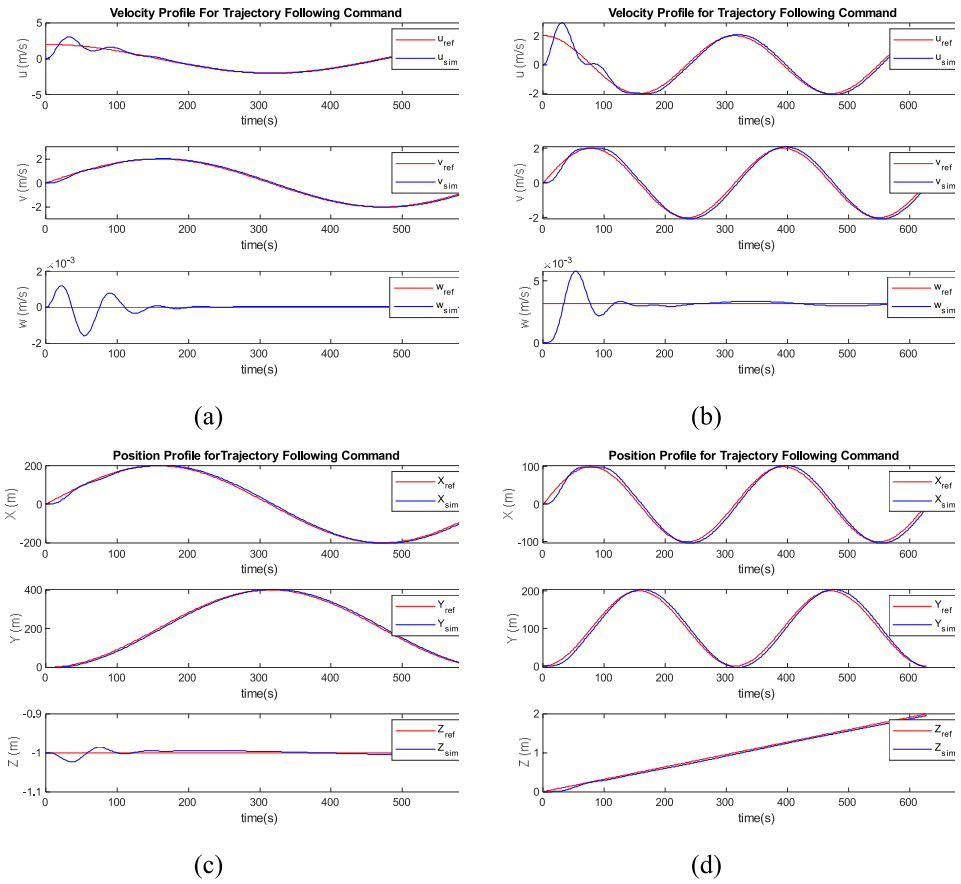


Fig. 13. Simulation result of trajectory following for (a) velocity profile of circular path; (b) velocity profile of spiral path; (c) position profile of circular path and (d) position profile of the spiral path.

Figure 13 depicts that deviation in simulation results occurs because the model requires time to resemble the command given. For instance, in Fig. 13 (a), the *u* and *w* responses oscillate for seconds before resembling the command given. For the spiral trajectory command in Fig. 13 (b) and (d), all of the velocity and position profiles differ from the command given at the beginning of the simulation. Control input response must be examined to ensure whether the configuration can be applied in the actual model. Figure 14 presents the control input response of the model.

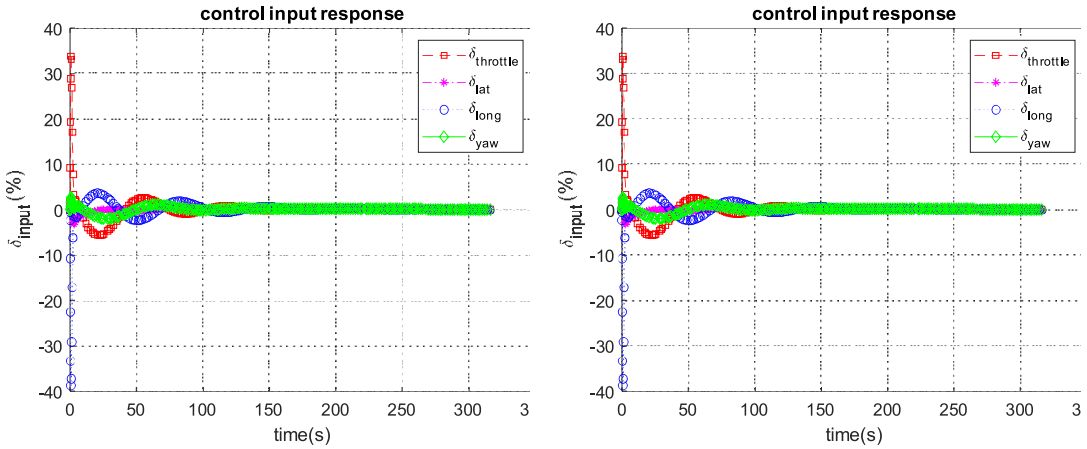


Fig. 14. Control input response of (a) circular path and (b) spiral path.

Based on Fig. 14, the response of all control inputs for both circular and spiral trajectories are within the limit of input capability. Therefore, the control system can be used in the actual model.

6. CONCLUSION

The quadrotor model has been constructed and integrated with parameter estimation to improve model accuracy. The nonlinear quadrotor model has undergone validation through flight tests, demonstrating behaviour similar to that of a quadrotor. A linear quadrotor model has been derived through linearization, closely resembling the nonlinear model.

An LQR control system has been designed to complement the existing stability augmentation system for trajectory following. This LQR approach has enhanced quadrotor flight performance by closely aligning with trajectory references, with only minor deviations observed at the beginning of the simulation.

The simulation results indicate that precise trajectory following control can be achieved using reasonable command inputs. This outcome undergoes the research contribution to advancing quadrotor control and highlights its practical relevance for applications requiring precise autonomous navigation.

REFERENCES

1. Erdelj, M., Natalizio, E., Chowdhury, K. R., & Akyildiz, I. F. (2017). Help from the Sky: Leveraging UAVs for Disaster Management. *IEEE Pervasive Comput.*, *16* (1), 24–32. DOI: 10.1109/MPRV.2017.11.
2. Shaffer, R., Karpenko, M., & Gong, Q. (2016). Unscented guidance for waypoint navigation of a fixed-wing UAV. In Proc. Am. Control Conf., (pp. 473–478). July 2016. DOI: 10.1109/ACC.2016.7524959.
3. Okyere, E., Bousbaine, A., Poyi, G. T., Joseph, A. K., & Andrade, J. M. (2019). LQR Controller Design for Quad-Rotor Helicopters. *J. Eng.*, *2019* (17), 4003–4007. DOI: 10.1049/joe.2018.8126.
4. Guardeño, R., López, M. J., & Sánchez, V. M. (2019). MIMO PID Controller Tuning Method for Quadrotor Based on LQR/LQG Theory. *Robotics*, *8* (2), 15–21. DOI: 10.3390/ROBOTICS8020036.
5. Priyambodo, T. K., Dhewa, O. A., & Susanto, T. (2019). Model of Linear Quadratic Regulator (LQR) Control System in Waypoint Flight Mission of Flying Wing UAV. *J. Telecommun. Electron. Comput. Eng. (JTEC), 12* (4), 2289–8131. Available at https://jtec.utem.edu.my/jtec/article/view/5696.
6. Shehzad, M. F., Bilal, A., & Ahmad, H. (2019). Position attitude control of an aerial robot (quadrotor) with intelligent PID and state feedback LQR controller: A comparative approach. In *Proc. 2019 16th Int. Bhurban Conf. Appl. Sci. Technol. (IBCAST 2019),* (pp. 340–346). 8–12 January 2019, Islamabad, Pakistan. DOI: 10.1109/IBCAST.2019.8667170.
7. Saraf, P., Gupta, M., & Parimi, A. M. (2020). A comparative study between a classical and optimal controller for a quadrotor. In *2020 IEEE 17th India Counc. Int. Conf. (INDICON2020)*. 10–13 December 2020. New Delhi, India DOI: 10.1109/INDICON49873.2020.9342485.
8. Islam, M., & Okasha, M. (2019). A comparative study of PD, LQR and MPC on quadrotor using quaternion approach. In *2019 7th Int. Conf. Mechatronics Eng. (ICOM 2019)*, (pp. 1–6). 30–31 October 2019, Putrajaya, Malaysia. DOI: 10.1109/ICOM47790.2019.8952046.
9. Rinaldi, M., Primatesta, S., & Guglieri, G. (2023). A Comparative Study for Control of Quadrotor UAVs. *Appl. Sci.*, *13* (6). DOI: 10.3390/app13063464.
10. Shakeel, T., Arshad, J., Jaffery, M. H., Rehman, A. U., Eldin, E. T., Ghamry, N. A., & Shafiq, M. (2022). A Comparative Study of Control Methods for X3D Quadrotor Feedback Trajectory Control. *Appl. Sci.*, *12* (18), 9254. DOI: 10.3390/app12189254.
11. Abdulghany, A. R. (2017). Generalization of Parallel Axis Theorem for Rotational Inertia. *Am. J. Phys.*, *85* (10), 791–795. DOI: 10.1119/1.4994835.
12. Zhou, L., Pljonkin, A., & Singh, P. K. (2022). Modeling and PID Control of Quadrotor UAV Based on Machine Learning. *J. Intell. Syst.*, *31* (1), 1112–1122. DOI: 10.1515/jisys-2021-0213.
13. Kabir, A. M. (2019). Autonomous Control of a Quadrotor-Manipulator Application of Extended State Disturbance Observer. *arXiv*.
14. Bouabdallah, S., Murrieri, P., & Siegwart, R. (2005). Towards Autonomous Indoor Micro VTOL. *Auton. Robots*, *18* (2), 171–183. DOI: 10.1007/s10514-005-0724-z.
15. Padfield, G. D. (2007). *Helicopter Flight Dynamics: The Theory and Application of Flying Qualities and Simulation Modelling* (2nd ed.). Oxford: Blackwell Publishing Ltd.
16. Roskam, J. (2018). *Airplane Flight Dynamics and Automatic Flight Controls: Part I* (8th ed.). DARcorporation.
17. Budiyono, A., & Wibowo, S. S. (2007). Optimal Tracking Controller Design for a Small Scale Helicopter. *J. Bionic Eng.*, *4* (4), 271–280. DOI: 10.1016/S1672-6529(07)60041-9.